Journal of the Korean Electrochemical Society
Vol. 5, No. 4, 2002, 178-182

Cycling Behavior of Binder-Free Graphite-Lithium Intercalation Anode in $AlCl_3$-EMIC-LiCl-$SOCl_2$ Room-Temperature Molten Salt

Nobuyuki Koura, Takuto Minami, Keiko Etoh, Yasushi Idemoto†, and Futoshi Matsumoto

Faculty of Science and Technology, Tokyo University of Science, 2641 Yamazaki, Noda, Chiba 278-8510, Japan

(Received June 22, 2002; Accepted October 8, 2002)

Abstract. The electrochemical behavior of binder-free carbon anode, comprising of only artificial and natural graphite (AG and NG) particles, for intercalation and deintercalation of lithium ion (Li^+) in aluminum chloride ($AlCl_3$)-1-ethyl-3-methylimidazolium chloride (EMIC)-lithium chloride (LiCl)-thionyl chloride ($SOCl_2$) room-temperature molten salt (RTMS) was studied. Binder-free carbon electrodes were fabricated using electrophoretic deposition (EPD) method. The binder-free carbon anodes provided a relatively flat charge and discharge potentials (0 to 0.2 V *vs.* Li/Li^+) and current capabilities (250~340 $mAh \cdot g^{-1}$) for the intercalation and deintercalation of Li^+. Stability of the binder-free carbon anodes for intercalation and deintercalation of 50 cycles was confirmed.

Key words : Room-temperature molten salt, Lithum secondary battery, Carbon anode

1. Introduction

Recently, room-temperature molten salts (RTMS) attract a great deal of attention as an electrolyte for lithium (Li) secondary batteries because it has several unique properties, such as a wide electrochemical window, high inherent conductivity, negligible vapor pressure, and nonflammability[1-3]. RTMS composed of aluminum chloride ($AlCl_3$) and 1-ethyl-3-methylimidazolium chloride (EMIC) has been used in the development of several primary and secondary batteries. Batteries such as Al anode/polyaniline powder cathode[4], Al anode/Cl_2 cathode[5], etc[6,7]. using the RTMS has been reported. Moreover, the addition of thionyl chloride ($SOCl_2$), H_2O, and HCl[2,3,8,9] into the RTMS had been found to extend the electrochemical potential window as far as Li can be deposited and stripped. The results have indicated that the development of Li batteries with RTMS is promising.

We have recently examined the electrochemical behavior of a graphite anode composed of only artificial graphite particles for intercalation and deintercalation of a lithium ion (Li^+) into and from graphites in $AlCl_3$-EMIC-LiCl RTMS containing $SOCl_2$ and confirmed that the intercalation and deintercalation of Li^+ occur with electrochemical and XRD measurements[10]. The binder-free graphite electrode was fabricated by us at first using the electrophoretic deposition (EPD) method[11]. Moreover, the intercalation and deintercalation could not be observed with the electrode composed of the mixture with various ratios of graphite and binder in the LiCl-saturated $AlCl_3$-EMIC RTMS containing $SOCl_2$. The EMI^+ reductive intercalation (0.5 V) into the graphites has also been reported in the $AlCl_3$-EMIC melt in the absence of $SOCl_2$[12]. Judging from these results, we considered that the intercalation and deintercalation of Li^+ in the LiCl-saturated $AlCl_3$-EMIC RTMS containing $SOCl_2$ were produced using the binder-free graphite electrode and by the addition of $SOCl_2$, and that the removal of the PVDF binder increases the wetting capabilities of the electrode surface by the melt. Further, a large amount of Li^+ can intercalate and deintercalate easily, and also the addition of $SOCl_2$ produces the surface layers which prevent the EMI^+ reductive intercalation into the graphite as well as the extension of an electrochemical window.

In this study, we examined cycling behavior for the electrochemical intercalation and deintercalation behavior of Li^+ into and from carbon anode composed of artificial and natural graphites (AG and NG) at constant-current electrolysis in $AlCl_3$ (60 mol%)-EMIC (40 mol%) RTMS containing LiCl and $SOCl_2$. The variations of the current capacity and efficiency for the electrochemical intercalation and deintercalation of Li^+ were compared at various current densities.

2. Experimental

EMIC was synthesized as previously reported[13]. $AlCl_3$ (60 mol%)-EMIC (40 mol%) RTMS was prepared by the addition of sublimed $AlCl_3$ to EMIC with stirring. The RTMS (colorless liquid) was purified using an Al substitution method[3]. An excess of anhydrous LiCl dried under a vacuum at 200°C for one week was added to the melt. Next, $SOCl_2$ was added into the LiCl-saturated $AlCl_3$-EMIC RTMS. A binder-free carbon electrode (1 cm^2) was used as the working electrode. Li foils (2 cm^2) were used as a reference and counter electrodes in the melts. Carbon particles, KS-25 (D%50 = 10 μm) and LF-18A (D%50 = 18 μm), were obtained from Timcal and Tyuuetsu cokuen kougyoushyo. The EPD bath was prepared

†E-mail: idemoto@rs.noda.tus.ac.jp

by suspending an carbon particle (5 g·l^{-1}) and triethylamine (1 ml·l^{-1}) in acetonitrile using an ultrasonic cleaner. The anode and cathode substrates used in the EPD were Mo and Pt, respectively. The deposition of carbon particles was done at 300 V for 30 s. The carbon particle covered the Mo current collector surface (1.8~2.2 mg·cm^{-2}) uniformly and its thickness was 60 μm[11]. All electrochemical experiments were performed using a computer-controlled electrochemical measuring system (HZ-3000, Hokuto Denko, Japan) and an automatic battery charging-discharging instrument (HJR-110mSM6, Hokuto Denko, Japan) under a purified Ar atmosphere at a vacuum atmosphere's dry box at 20± 2°C.

3. Results and Discussion

Figure 1 shows a typical cyclic voltammogram obtained with a binder-free AG electrode in the LiCl-saturated $AlCl_3$ (60 mol%)-EMIC (40 mol%) RTMS containing 0.11 mol· dm^{-3} $SOCl_2$ at 200 μVs^{-1}. In the potential region from 0 to 0.25 V, three coupled redox peaks were observed and these peak currents reached a steady-state after the 10th cycle. When the electrode potential was held at 15 mV, the electrode surface exhibited a golden-yellow color. The electrochemical behavior in the potential region from 0 to 0.25 V was very similar to the one observed in EC-DMC (1 : 3)/ $LiAsF_6$ with a graphite-lithium intercalation anode composed of AG and a binder (polyvinylidene fluoride (PVDF))[14]. It is well-known that the representative three coupled redox peaks, indicating the phase transitions between Li^+ intercalation stages, were observed in the organic solvent containing Li salt. The first, second, and third stages were identified as a stage for the formation of the structure composed of LiC_6, $Li_{0.5}C_6$, and $Li_{0.16}C_6$, respectively. A surface of graphite electrode intercalated stepwise to LiC_6 also shows a golden-yellow color[15]. In comparison with the results obtained from the graphite electrode, composed of AG and PVDF, in organic solution, it can be postulated that the intercalation and deintercalation of Li^+ into and from the binder-free graphite anode occur in the $AlCl_3$-EMIC-LiCl-$SOCl_2$ RTMS. Moreover, irreversible reduction peak current was observed at 2.8 V (vs. Li/Li^+) and a smaller reduction current was observed in the potential region from 0.3 to 2.5 V at the first cycle. With the following potential scan, these reduction currents decreased (Fig. 1, inset). The reduction peak current observed at 2.8 V at the first potential scan can be assigned to the reduction of $SOCl_2$.[16] The reduction current observed in the potential region from 0.3 to 2.5 V may be due to the formation of the surface electrolyte interphase (SEI).

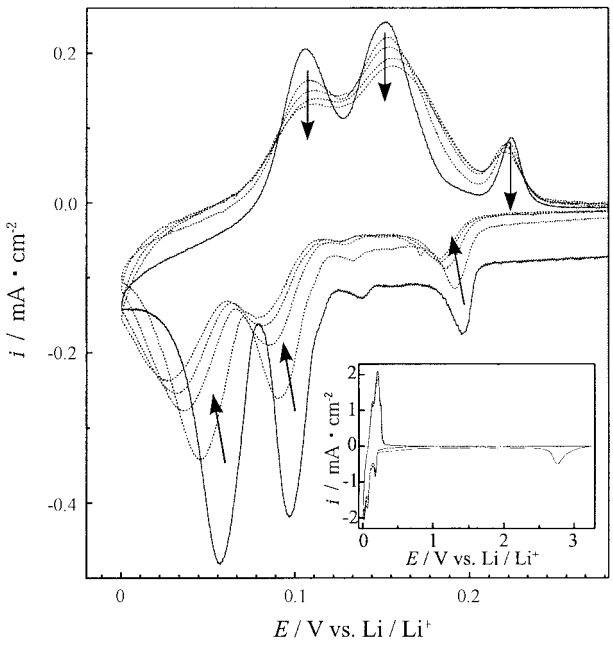

Fig. 1. Typical voltammetric behavior of a binder-free AG anode from 0 to 2.8 V at 200 μV·s^{-1} in the LiCl-saturated $AlCl_3$ (60 mol%)-EMIC (40 mol%) melt containing 0.11 mol·dm^{-3} $SOCl_2$. The binder-free anode was prepared with AG (KS-25, 1.8 mg·cm^{-2} on Mo). Electrolyte temp.: 20°C. The inset shows the cyclic voltammogram in the same condition from 0 to 3.3 V.

A representative intercalation-deintercalation cycling of Li^+ obtained with the binder-free AG anode at a constant-current electrolysis in the LiCl-saturated $AlCl_3$ (60 mol%)-EMIC (40 mol%) RTMS containing 0.11 mol·dm^{-3} $SOCl_2$ are shown in Figure 2. The reduction was done at the first cycle in the rate of (a) 0.3 (0.28 mA·cm^{-2}) and (b-d) 0.5 C. The following reduction was done in the rate of 0.1 C. The oxidation was done in the rate of (a, b) 0.1, (c) 0.2, and (d) 0.3 C. Potential vs. reduction capacity curves at the first cycle in all the oxidation-reduction rates were quite different from those at the following cycles. The curves were composed of several sloping and plateau regions and showed the electrode potentials from 0 to 2.5 V. The region composed of several slopings and plateaus became narrower by increasing the reduction rate at the first cycle (Fig. 2(a) and (b)). The reason for the appearance of a higher potential than the one for the intercalation of Li^+ is that the applied constant current is consumed by the reduction of $SOCl_2$ and the formation of the SEI. The reduction capacity at the first cycle exceeded the theoretical capacity of graphite (372 mAh·g^{-1}) and reached 450~920 mAh·g^{-1}. The excess of the reduction capacity at the first cycle is due to the additional capacity of the $SOCl_2$ reduction and the SEI formation. Therefore, the oxidation capacity at the first cycle is only 180~230 mAh·g^{-1}, indicating the deintercalation of Li^+ from the AG anode. After the first cycle, the potential vs. capacity curves for the reduction and oxidation clearly showed three phase transitions between the intercalation stages in the potential region from 0 to 0.25 V. The excess of capacity due to the formation of the SEI (0.3~0.6 V) decreased as the cycle progressed and the reduction capacity approached the theoretical capacity of graphite. On the other hand, the oxidation capacity increased as the cycles progressed. As a result, at the 50th cycle, capacities for the reduction and oxidation, and the reduction-oxidation efficiency reached 245~335, 225~300 mAh·g^{-1}, and 88~93%, respectively (Fig. 3). Unfortunately, an increase of the oxidation rate caused the undue deterioration of the current capacity, although the reaction efficiency almost did not change in all the oxidation rate (Fig. 3(b-d)). The rapid expansion and

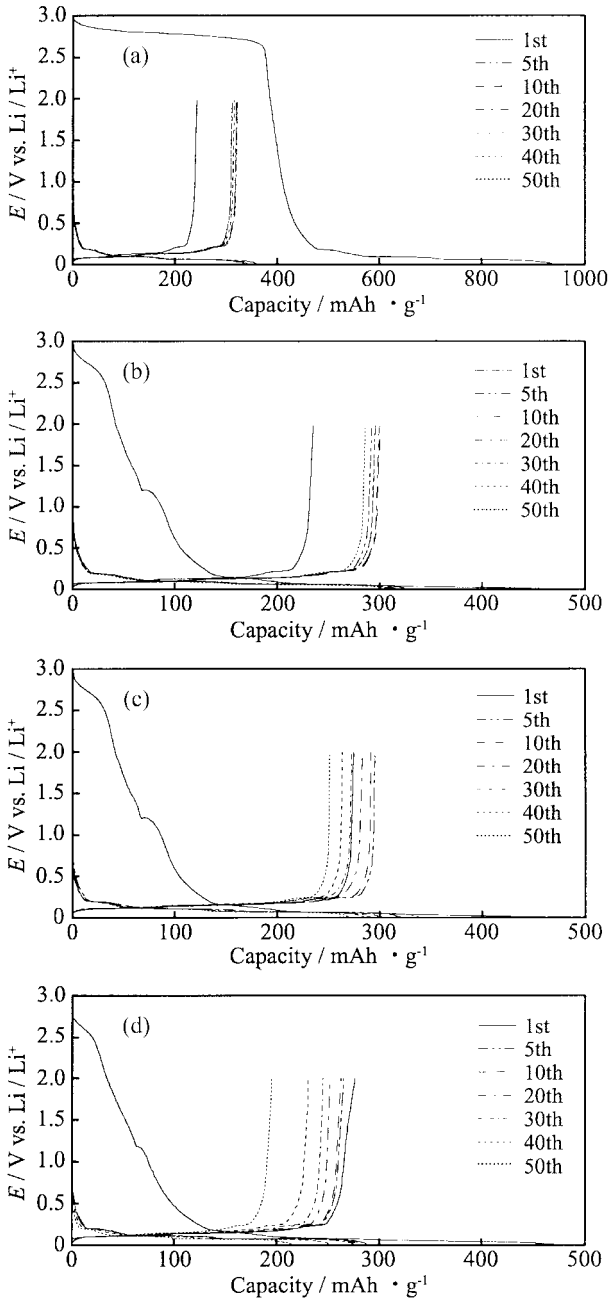

Fig. 2. Reduction/oxidation cycles obtained with the binder-free AG anode (KS-25, 1.8 mg·cm^{-2} on Mo) in the LiCl-saturated $AlCl_3$ (60 mol%)-EMIC (40 mol%) melt containing 0.11 mol·dm^{-3} $SOCl_2$. The graphite anode was reduced at the first cycle in the rate of (a) 0.3 (0.28 mA·cm^{-2}) and (b-d) 0.5 C. The following reduction was done in the rate of 0.1 C. The oxidation was done in the rate of (b) 0.1, (c) 0.2, and (d) 0.3 C. The graphite anode was not allowed to stand for anytime before charging and discharging. Electrolyte temp.: 20°C.

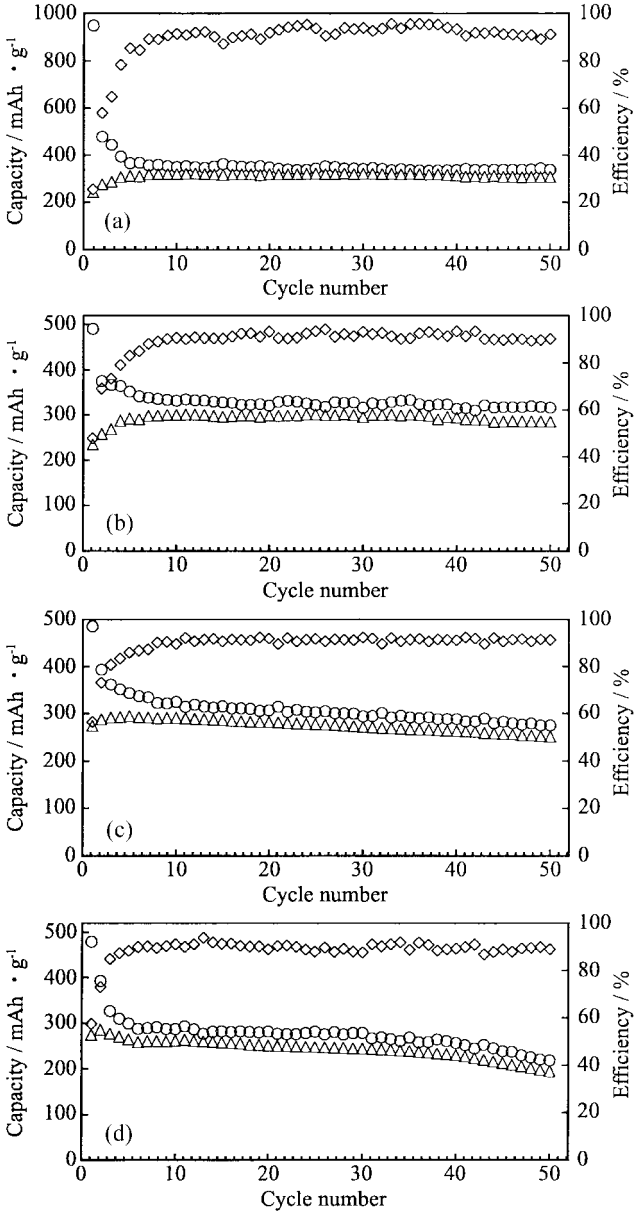

Fig. 3. Changes in the reduction/oxidation efficiency (◇) and capacities for the reduction (○) and oxidation (△) of the binder-free AG anode. The following reduction was done in the rate of 0.1 C. The oxidation was done in the rate of (b) 0.1, (c) 0.2, and (d) 0.3 C. The experimental conditions are the same as those in Figure 2.

contraction of the graphite layer with a rapid reduction and oxidation might cause a drop of a small amount of graphite particles from the carbon anode. Improvement of durability against the rapid expansion and contraction of the carbon layer is expected. EPD for obtaining carbon anode containing small amount of binder is examined now.

Figure 4 shows a representative intercalation-deintercalation cycling of Li^+ obtained with the binder-free NG anode at a constant-current electrolysis in the LiCl-saturated $AlCl_3$ (60 mol%)-EMIC(40 mol%) RTMS containing 0.11 mol·dm^{-3} $SOCl_2$. The reduction was done at the first cycle in the rate of 0.5 C (0.47 mA·cm^{-2}) and the following reduction were done in the rate of 0.1 C. The oxidation were done in the rate of 0.1 C. Also, in the NG anode, several sloping and plateau regions were observed from 0 to 2.5 V at the first reduction. The reason for the appearance of a higher potential than the one for the intercalation of Li^+ may be that the applied constant current is consumed by the reduction of

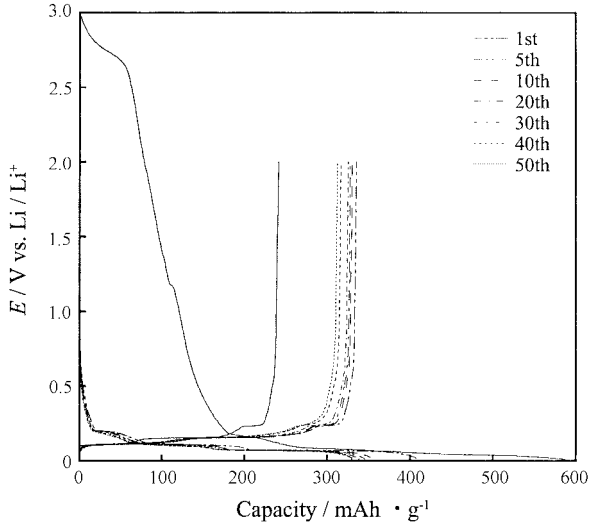

Fig. 4. Reduction/oxidation cycles obtained with the binder-free NG electrode (LF-18A, 1.8 mg·m^{-2} on Mo) in the LiCl-saturated $AlCl_3$ (60 mol%)-EMIC (40 mol%) melt containing 0.11 mol·dm^{-3} $SOCl_2$. The graphite anode was reduced at the first cycle in the rate of 0.5 C. The following reduction was done in the rate of 0.1 C. The oxidation was done in the rate of 0.1 C. The graphite anode was not allowed to stand for anytime before charging and discharging. Electrolyte temp.: 20°C.

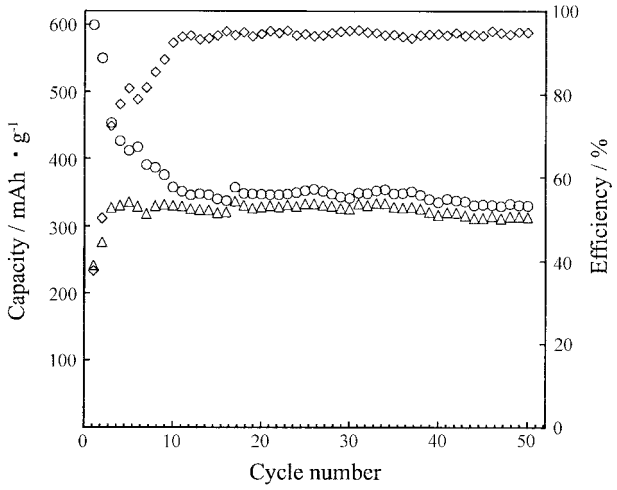

Fig. 5. Changes in the reduction/oxidation efficiency (◇) and capacities for the reduction (○) and oxidation (△) of the binder-free NG anode. The experimental conditions are the same as those in Figure 4.

$SOCl_2$ and the formation of the SEI, similar to the one with the binder-free AG anode. In the case of a lower reduction rate than 0.5 C at the first cycle, the electrode potential was kept at the reduction potential of $SOCl_2$. The reduction capacity at the first cycle reached 600 mAh·g^{-1}. The oxidation capacity at the first cycle is only 230 mAh·g^{-1}, indicating the deintercalation of Li^+ from the NG anode. After the first cycle, the potential vs. capacity curves for the reduction and oxidation showed three clear phase transitions between the intercalation stages in the potential region from 0 to 0.2 V. The excess of capacity due to the formation of the SEI (around 0.3 V) decreased as the cycle progressed. On the other hand, the oxidation capacity increased as the cycles progressed. As a result, at the 50th cycle, capacities for the reduction and oxidation, and the reduction-oxidation efficiency reached 330, 320 mAh·g^{-1}, and 95%, respectively (Fig. 5). The capacities for the reduction and oxidation, and the reduction-oxidation efficiency obtained with NG anode were larger than those observed with AG. The current capacities for the reduction and oxidation, and efficiency at NG anode approached to theoretical capacity of graphite closely. Using NG particles brought out the improvement in the current capacities and efficiency. Compared with the density and the state of aggregation of AG and NG particles on the Mo substrate, the reason for the improvement of current capacities and efficiency with NG particles is considered now.

The electrochemical behavior of the binder-free NG anode resembled the one observed with binder-free AG anode very closely. Intercalation and deintercalation could not also be observed with the electrode composed of the mixture with various ratios of NG and binder in the $AlCl_3$-EMIC-LiCl-$SOCl_2$ RTMS. The intercalation and deintercalation of Li^+ into and from the NG in the $AlCl_3$-EMIC-LiCl-$SOCl_2$ RTMS were also produced by using the binder-free anodes. Moreover, we consider that the removal of the PVDF binder causes the penetration of the melt into the gaps between carbon particles and that Li^+ can intercalate into and deintercalate from graphite paticles easily. Elucidation of the mechanism of the diffusion of Li^+ in graphite film is now under way. The results obtained from AG and NG anodes indicated that the binder-free anode using the EPD method is useful in the fabrication of an electrode for Li ion secondary batteries, which operate in the $AlCl_3$-EMIC-LiCl-$SOCl_2$ RTMS. Anode and cathode fabricated by EPD with various carbon and transition metal oxide materials are expected to operate in various RTMS.

4. Conclusion

Binder-free carbon anodes were fabricated by the EPD method with AG and NG particles. Electrochemical behavior of the anodes for intercalation and deintercalation of Li^+ in the $AlCl_3$-EMIC-LiCl-$SOCl_2$ RTMS was investigated by cyclic voltammetry and constant-current charge-discharge testing. Cyclic voltammograms and the potential vs. capacity curves for the reduction and oxidation showed three clear phase transitions between the Li^+ intercalation stages in the potential region from 0 to 0.2 V. Although the reduction capacity at the first cycle exceeded the theoretical capacity of graphite (372 mAh·g^{-1}) and reached 450~920 mAh·g^{-1} due to the addition of the reduction of $SOCl_2$ and the formation of SEI, the potential vs. capacity curves for the reduction and oxidation showed stable charge and discharge potentials after several cycles. The stable charge and discharge potentials were kept for 50 cycles. At the 50th cycle, current capacities for the reduction and oxidation, and efficiencies at AG and NG cathodes reached 245~335, 225~320 mAh·g^{-1}, and 88

~95%, respectively. The current capacities for the reduction and oxidation, and efficiencies at NG anode approached to theoretical capacity. From these results, it was indicated that the binder-free anode using the EPD method is useful in the fabrication of an electrode for Li ion secondary batteries, which operate in the $AlCl_3$-EMIC-LiCl-$SOCl_2$ RTMS and the development of Li ion secondary batteries with the RTMS is promising.

References

1. C. S-Kelley and R. T. Carline, *J. Electrochem. Soc.*, **141**, 873 (1994).
2. J. Fuller, R. A. Osteryoung, and R. T. Carlin, *J. Electrochem. Soc.*, *142*, 3632 (1995).
3. N. Koura, K. Iizuka, Y. Idemoto, and K. Ui, *Electrochemistry*, **67**, 706 (1999).
4. N. Koura, H. Ejiri, and K. Takeishi, *J. Electrochem. Soc.*, **140**, 602 (1993).
5. P. R. Gifford and J. B. Palmisano, *J. Electrochem. Soc.*, **135**, 650 (1988).
6. G. F. Reynolds, Jr. C. J. Dymek, and J. S. Wikes, *J. Power Source*, **15**, 109 (1985).
7. S. Takahashi, N. Koura, and R. Nakajima, *Denki Kagaku*, **54**, 263 (1986).
8. T. L. Riechel and J. S. Wilkes, *J. Electrochem. Soc.*, **139**, 977 (1992).
9. J. Fuller, R. T. Carlin, and R. A. Osteryoung, *J. Electrochem. Soc.*, **144**, 3881 (1997).
10. N. Koura, K. Etoh, Y. Idemoto, and F. Matsumoto, *Chemistry Letters*, **1320** (2001).
11. N. Koura, H. Tsuiki, N. Terakura, Y. Idemoto, F. Matsumoto, K. Ui, K. Yamada, and T. Mitate, *Hyomen Gijutsu*, **52**, 143 (2001).
12. R. T. Carlin, J. Fuller, W. K. Kuhn, M. J. Lysaght, and P. C. Trulove, *J. Appl. Electrochem.*, **26**, 1147 (1996).
13. J. S. Wilkes, J. A. Levisky, R. A. Wilson, and C. L. Hussey, *Inorg. Chem.*, **21**, 1263 (1982).
14. D. Aurbach, B. Markovsky, I. Weissman, E. Levi, and Y. Ein-Eli, *Electrochim. Acta*, **45**, 67 (1999).
15. Z. Jiang, M. Alamgir, and K. M. Abraham, *J. Electrochem. Soc.*, **142 (2)**, 333 (1995).
16. J. Fuller and R. T. Carlin, *Electrochem. Soc. Proceeding*, **7**, 372 (1996).